Molecular Alignment within β-Sheets in A$\beta_{14\text{-}23}$ Fibrils: Solid-State NMR Experiments and Theoretical Predictions

Zimei Bu,* Yuan Shi,† David J. E. Callaway,*† and Robert Tycko‡
*Fox Chase Cancer Center, Philadelphia, Pennsylvania; †New York University School of Medicine, New York, New York; and ‡Laboratory of Chemical Physics, National Institute of Diabetes and Digestive and Kidney Diseases, National Institutes of Health, Bethesda, Maryland

ABSTRACT We report investigations of the molecular structure of amyloid fibrils formed by residues 14–23 of the β-amyloid peptide associated with Alzheimer's disease (A$\beta_{14\text{-}23}$), using solid-state nuclear magnetic resonance (NMR) techniques in conjunction with electron microscopy and atomic force microscopy. The NMR measurements, which include two-dimensional proton-mediated ^{13}C-^{13}C exchange and two-dimensional relayed proton-mediated ^{13}C-^{13}C exchange spectra, show that A$\beta_{14\text{-}23}$ fibrils contain antiparallel β-sheets with a registry of backbone hydrogen bonds that aligns residue $17+k$ of each peptide molecule with residue $22-k$ of neighboring molecules in the same β-sheet. We compare these results, as well as previously reported experimental results for fibrils formed by other β-amyloid fragments, with theoretical predictions of molecular alignment based on databases of residue-specific alignments in antiparallel β-sheets in known protein structures. While the theoretical predictions are not in exact agreement with the experimental results, they facilitate the design of experiments by suggesting a small number of plausible alignments that are readily distinguished by solid-state NMR.

INTRODUCTION

Amyloid fibrils are filamentous aggregates formed by a large class of peptides and proteins with diverse amino-acid sequences. Current interest in amyloid fibrils arises from their involvement in amyloid diseases (including Alzheimer's disease, type 2 diabetes, dialysis-related amyloidosis, Parkinson's disease, transthyretin amyloidoses, transmissible spongiform encephalopathy, and others (1)), from the fairly recent realization that the propensity to form amyloid fibrils is not restricted to disease-associated peptides and proteins (but is instead a nearly generic property of polypeptides (2)), and from the possibility that amyloid fibrils may be a useful basis for development of self-assembled nanomaterials (3,4). Knowledge of the molecular-level details of amyloid fibril structures would contribute to our understanding of potential mechanisms by which amyloid fibrils contribute to or cause amyloid diseases, to the development of therapeutic agents (5–7), to our understanding of the intermolecular and intramolecular interactions that stabilize amyloid fibrils, and possibly to the development of amyloid-based nanomaterials. These molecular-level structural details are only recently becoming accessible, largely through the application of modern solid-state nuclear magnetic resonance (NMR) techniques such as multiple quantum NMR (8–10), dipolar recoupling (11–21), and various forms of multidimensional spectroscopy (10,18,19,22–26) in conjunction with magic-angle spinning (MAS). Solid-state NMR measurements have revealed that amyloid fibrils, which are known to be primarily β-sheet structures from x-ray fiber diffraction patterns (27–29), can contain either parallel or antiparallel β-sheets, depending on the amino-acid sequence. To date, antiparallel β-sheets have only been observed in fibrils formed by relatively short peptides that contain one β-strand segment (10,12,19). The precise registry of backbone hydrogen bonds (i.e., the alignment of neighboring β-strands within a single β-sheet) can be pH-dependent (19) and is not fully determined by the local amino acid sequence (e.g., by seven-residue segments). Not all short peptides form antiparallel β-sheets in amyloid fibrils (20,30), and the β-sheets in fibrils formed by short peptides can be switched from antiparallel to parallel by attachment of N-terminal alkyl chains (31).

Techniques other than solid-state NMR have also contributed greatly to our developing understanding of amyloid structures. These techniques include electron microscopy (32–36), x-ray crystallography (30,37), electron paramagnetic resonance (38–42), hydrogen/deuterium exchange (25,43–47), chemical cross-linking (13,48), limited proteolysis (49,50), and scanning mutagenesis (51–53). Results from these techniques are generally consistent with those from solid-state NMR, especially with regard to the types of β-sheets contained in amyloid fibrils.

In this article, we report the results of solid-state NMR measurements on fibrils formed by residues 14–23 of the full-length β-amyloid peptide associated with Alzheimer's disease (A$\beta_{14\text{-}23}$, sequence Ac-HQKLVFFAED-NH_2, with acetyl and amide capping groups at the N- and C-termini). We have chosen to study A$\beta_{14\text{-}23}$ for the following reasons:

1. In earlier work, Tjernberg et al. (54) examined amyloid fibril formation by β-hairpin peptides containing the A$\beta_{14\text{-}23}$ sequence on both sides of a type 1′ β-turn, constrained to align either residue $17+k$ with residue $20-k$ or residue $17+k$ with residue $21-k$ (54). Both β-hairpin peptides were found to form fibrils, raising the question of what

Submitted June 8, 2006, and accepted for publication October 2, 2006.

Address reprint requests to R. Tycko, E-mail: robertt@niddk.nih.gov; or D. Callaway, david.callaway@fccc.edu.

0006-3495/07/01/594/09 $2.00

doi: 10.1529/biophysj.106.091017

alignment is preferred by the unconstrained $A\beta_{14\text{-}23}$ peptide in amyloid fibrils (including the possibility of either antiparallel or parallel β-sheet structure).

2. Although the hexapeptide Ac-KLVFFAE-NH_2 has been shown to form amyloid fibrils (10), other β-amyloid-derived peptides containing the LVFFA hydrophobic segment and a total of nine or fewer residues were found by Tjernberg et al. not to form fibrils (55), while all peptides examined that contained 11 or more residues did form fibrils (19,55). Residues 14–23 may therefore be considered the minimal segment of the β-amyloid sequence that is sufficient for fibril formation.
3. Given that our current understanding of amyloid structures and the interactions that stabilize these structures is relatively primitive (e.g., compared with our understanding of soluble, monomeric, globular protein structures), structural studies of model systems such as $A\beta_{14\text{-}23}$ fibrils are expected to contribute important information about the variety and sequence dependence of amyloid structures and stabilizing interactions.
4. Model systems such as $A\beta_{14\text{-}23}$ fibrils serve as test-beds for the development and demonstration of experimental methods for determining specific features of amyloid structures and theoretical methods for predicting these structural features.

The solid-state NMR measurements described below show that $A\beta_{14\text{-}23}$ fibrils contain antiparallel β-sheets with hydrogen-bond registry that aligns residue $17+k$ with residue $22-k$, for integral k (e.g., V18 of each $A\beta_{14\text{-}23}$ molecule forms hydrogen bonds with A21 of a neighboring molecule in the same β-sheet). Moreover, the solid-state NMR data indicate a high level of order in the β-sheets, with no detectable defects in the $17+k \leftrightarrow 22-k$ hydrogen-bond registry. We compare these experimental results with theoretical predictions of β-strand alignment. In particular, we show that simple predictive tools based upon comparisons with known protein structures may be useful in guiding experimental design, although precise prediction of registry may not be possible.

METHODS

Peptide synthesis and fibril formation

Isotopically labeled amino acids were obtained from Cambridge Isotope Laboratories (Andover, MA). $A\beta_{14\text{-}23}$ peptides containing labeled amino acids were synthesized on a Symphony/Multiplex solid-phase synthesizer (Protein Technologies, Tucson, AZ), using standard FMOC synthesis and cleavage protocols. Peptides were purified by high performance liquid chromatography using two mobile phases, water with 0.1% trifluoroacetic acid and acetonitrile with 0.1% trifluoroacetic acid, on a C18 reverse phase column (Grace Vydac, Hesperia, CA). Final purity was >95%, as confirmed by a Kompact MALDI TOF mass spectrometer (Kratos, Chestnut Ridge, NY). After lyophilization of the high performance liquid chromatography fraction containing these peptides, $A\beta_{14\text{-}23}$ was dissolved at 5.3 mg/ml in 10 mM phosphate buffer, 0.01% NaN_3, at pH 4.7. Fibrils formed within three weeks at room temperature. $A\beta_{14\text{-}23}$ fibril samples were prepared with uniform ^{13}C and ^{15}N labeling of L17 and F20 (17,20-$A\beta_{14\text{-}23}$), V18 and F20 (18,20-$A\beta_{14\text{-}23}$), V18 and A21 (18,21-$A\beta_{14\text{-}23}$), and L17 and A21 (17,21-$A\beta_{14\text{-}23}$).

Electron microscopy and atomic force microscopy

Fibril formation was confirmed and fibril dimensions were determined using electron microscopy (EM) and atomic force microscopy (AFM). For EM measurements, 10 μl aliquots of incubated $A\beta_{14\text{-}23}$ solutions were placed on specimen grids covered by a formvar/carbon support film. Excess fluid was wicked off after 2 min and the grids were negatively stained with 4 mg/ml uranyl acetate in water. The stained grids were then examined and photographed with a JEOL (Tokyo, Japan) JEM-100CXII transmission electron microscope.

For AFM, fibrils were diluted in 0.5% acetic acid (pH 3) to a peptide concentration of ~0.5 mM. Both lyophilized and fully hydrated (i.e., never lyophilized or dried after incubation) fibrils were examined. A 50 μl aliquot was placed on freshly cleaved mica (1 cm^2 area), allowed to adsorb for several minutes, and drained from the mica surface. The surface was washed twice with 100 μl of 0.5% acetic acid, then dried under a stream of nitrogen gas. AFM images were obtained in air with a MultiMode AFM system (Veeco Instruments, Santa Barbara, CA) in tapping mode, using microactuated probes with a nominal force constant of 3 N/m and a nominal tip radius of curvature of 10 nm. Approximately 100 images of 5 μm × 5 μm areas were recorded for both lyophilized and hydrated samples, with 1024 pixel resolution in each lateral dimension. AFM images in Fig. 1 *b* are portions of typical 5 μm × 5 μm areas.

Solid-state NMR

NMR measurements were carried out at a magnetic field of 14.1 T (150.7 MHz ^{13}C NMR frequency) using Varian (Palo Alto, CA) Infinity and InfinityPlus spectrometer consoles and a Varian MAS probe with 3.2 mm MAS rotor diameters and 11 μl maximum sample volumes. Additional Teflon plugs were inserted in the rotors to restrict smaller samples to the center of the radio-frequency (rf) coil in the NMR probe. $A\beta_{14\text{-}23}$ fibril samples were pelleted in a microfuge (18,000 × g for 15 min), resuspended

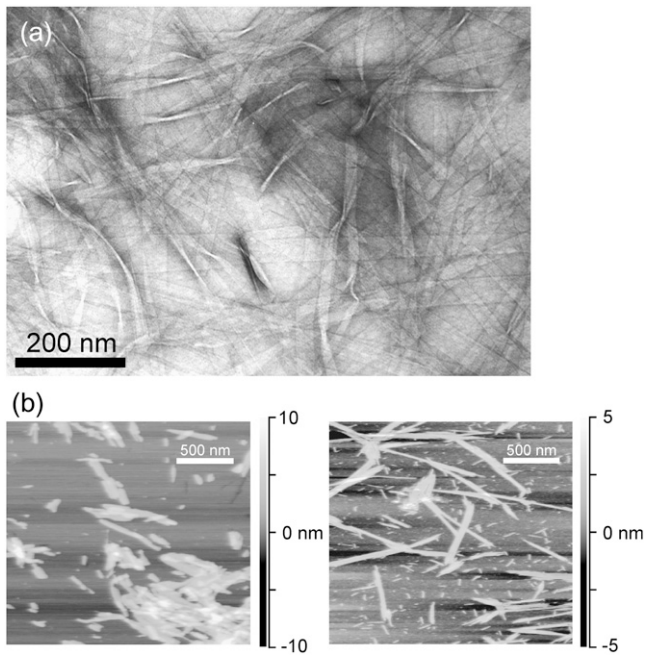

FIGURE 1 (*a*) Transmission electron microscope image of $A\beta_{14\text{-}23}$ fibrils, with negative staining. (*b*) Atomic force microscope images of $A\beta_{14\text{-}23}$ fibrils with (*left*) and without (*right*) lyophilization before dilution in 0.5% acetic acid and deposition on mica. Grayscales indicate height.

in deionized H_2O, and lyophilized before packing into MAS rotors. Sample quantities were in the 2–6 mg range. Lyophilization permitted the use of small sample volumes with concomitantly high MAS speeds, rf field amplitudes, and NMR sensitivity. As shown by AFM images (Fig. 1 *b*), lyophilization breaks A$\beta_{14\text{-}23}$ fibrils into 100-500 nm segments but does not otherwise affect fibril morphology. For certain measurements (specified below), lyophilized samples were rehydrated by addition of 2–3 μl of deionized H_2O.

Rf pulse sequences used in solid-state NMR measurements are shown in Fig. 2. One-dimensional ^{13}C NMR spectra (Fig. 2 *a*) were recorded with cross-polarization (CP) from protons (56) and with two-pulse phase-modulated proton decoupling (57). Decoupling fields were 110 kHz. ^{13}C rf fields were ~50 kHz during CP, with tangent-shaped amplitude modulation. Two-dimensional proton-mediated ^{13}C-^{13}C NMR exchange (2D-PME) spectra were recorded as described previously (19,58), using 150 μs CP periods, 200 μs proton spin diffusion (SD) periods in the exchange period, and MAS frequencies of 20.0–21.4 kHz (Fig. 2 *b*). Under these conditions, strong crosspeaks are observed between the NMR lines of ^{13}C pairs with directly-bonded protons for which the proton-proton distances are <3 Å. In particular, strong intermolecular crosspeaks between NMR lines of ^{13}C-labeled α-carbons (C_α) are detected when the corresponding residues are aligned in antiparallel β-sheets, leading to intermolecular distances of ~2.2 Å between α-protons (H_α). Thus, the presence or absence of particular C_α/C_α crosspeaks in 2D-PME spectra can be used to determine hydrogen-bond registry in antiparallel β-sheets (19,58).

C_α chemical shifts for L17 and F20 were found to be similar (0.7 ppm difference), preventing the observation of C_α/C_α crosspeaks in 2D-PME spectra of 17,20-A$\beta_{14\text{-}23}$ fibrils even if L17 and F20 were aligned in antiparallel β-sheets. Therefore, a new solid-state NMR technique was designed in which alignment of uniformly ^{13}C-labeled residues could be detected as an intermolecular crosspeak between carbonyl (CO) NMR lines. In this technique, called two-dimensional relayed proton-mediated ^{13}C-^{13}C NMR exchange (2D-RPME) spectroscopy (Fig. 2 *c*), ^{13}C spin polarization is transferred between CO sites during the exchange period in five steps:

1. A short ^{13}C-^{13}C dipolar recoupling period for intraresidue CO→C_α transfer.
2. A short CP period for one-bond $C_\alpha \rightarrow H_\alpha$ transfer.
3. A short proton SD period for intermolecular $H_\alpha \rightarrow H_\alpha$ transfer.
4. A second short CP period for one-bond $H_\alpha \rightarrow C_\alpha$ transfer.
5. A second short ^{13}C-^{13}C dipolar recoupling period for intraresidue $C_\alpha \rightarrow$ CO transfer. CP and SD conditions are the same as in 2D-PME measurements.

^{13}C-^{13}C dipolar recoupling periods employed the radio-frequency-driven recoupling pulse sequence (59,60), with one 8.0 μs ^{13}C π-pulse per MAS rotation period for a total of 16 rotation periods (1.067 ms at a 15.0 kHz MAS frequency). ^{13}C π-pulse phases followed the XY-16 pattern (61).

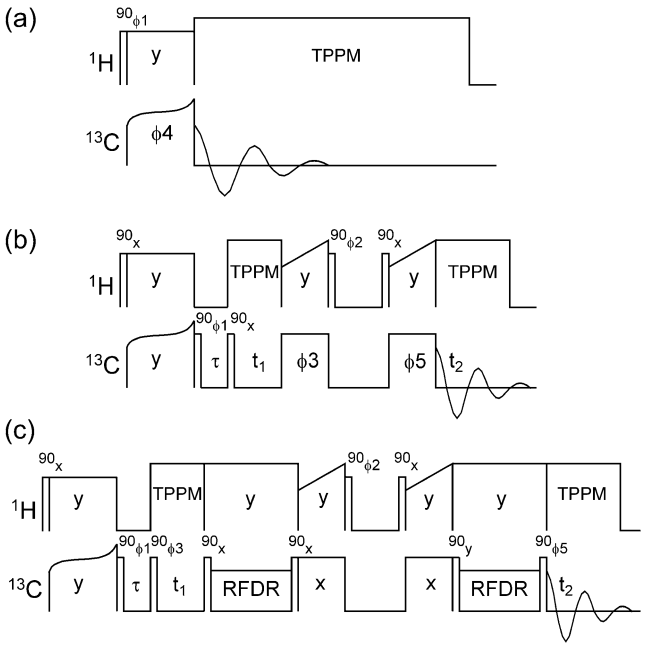

FIGURE 2 Radio-frequency pulse sequences for one-dimensional ^{13}C MAS NMR measurements (*a*), 2D-PME measurements (*b*), and 2D-RPME measurements (*c*). Radio-frequency-driven recoupling periods consist of one ^{13}C π pulse per MAS rotor period. Dephasing delays τ are 1 ms. Phase cycles are: $\phi1 = x, -x$; $\phi2 = x, x, -x, -x$; $\phi3 = x$ or y for real or imaginary signals in t_1; $\phi4 = x, x, y, y, -x, -x, -y, -y$; $\phi5 = x, x, x, x, y, y, y, y, -x, -x, -x, -x, -y, -y, -y, -y$. Receiver phase cycles are $x, -x, y, -y, -x, x, -y, y$ in panel *a* and $x, -x, -x, x, y, -y, -y, y, -x, x, x, -x, -y, y, y, -y$ in panels *b* and *c*.

RESULTS

Electron microscopy and atomic force microscopy

The EM image in Fig. 1 *a* shows that A$\beta_{14\text{-}23}$ forms fibrils with an apparently flat, ribbonlike morphology, with fibril widths of ~30 nm. Fibril widths exceed the 3.5 nm length of a single A$\beta_{14\text{-}23}$ molecule in a fully extended β-strand conformation, suggesting that each fibril contains many finer filaments with cross-β structures.

The AFM images in Fig. 1 *b* show that lyophilization breaks long A$\beta_{14\text{-}23}$ fibrils into shorter fragments, which tend to coalesce into clumps under the conditions of AFM measurements, but otherwise has no detectable effect on fibril morphology. Apparent fibril heights in AFM images of both lyophilized and hydrated fibrils are 2.5 ± 0.5 nm. The fibril heights may correspond to the thickness of between two and four β-sheets in a laminated cross-β structure.

Solid-state NMR

Fig. 3 shows one-dimensional ^{13}C MAS NMR spectra of the four A$\beta_{14\text{-}23}$ fibril samples examined in this work. ^{13}C chemical shift assignments, summarized in Table 1, are based on the known chemical shift ranges for individual carbon sites in amino acids, and are confirmed by the 2D-NMR spectra described below. Chemical shifts for CO, C_α, and β-carbon (C_β) sites are consistent with a β-strand conformation for residues 17–21 in A$\beta_{14\text{-}23}$ fibrils (i.e., upfield secondary shifts relative to random coil values (62) for CO and C_α, downfield secondary shifts for C_β). Only the C_α line for L17 does not show a strong secondary shift. In the dry, lyophilized state, ^{13}C MAS NMR line-widths for resolved single sites are 1.5 to 2.1 ppm (full width at half-maximum). In the rehydrated state (Fig. 3, *a* and *b*, *bottom spectra*), line-widths are 1.0 ppm. The reduction of ^{13}C MAS NMR line-widths upon rehydration is attributable to increased molecular motion, which partially averages out the inhomogenous broadening that arises from structural variations within these noncrystalline fibril samples. Structural variations that may contribute to the observed

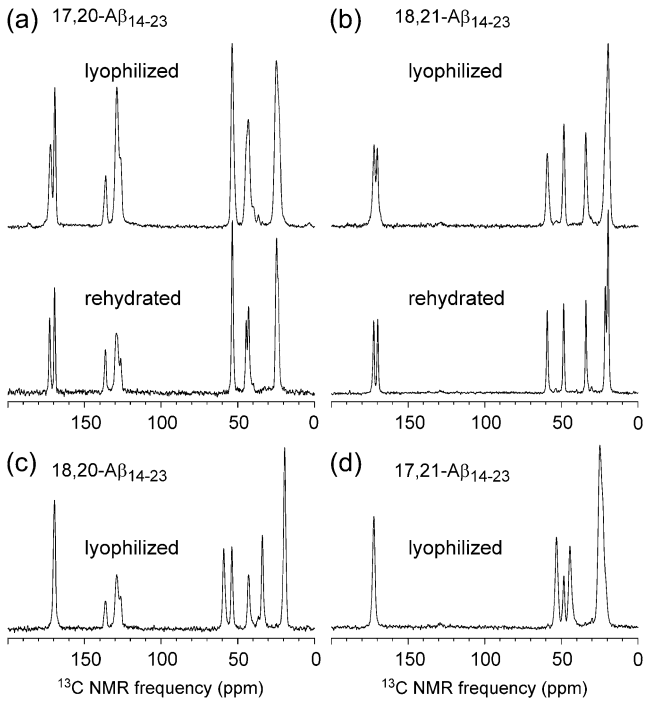

FIGURE 3 One-dimensional ^{13}C MAS NMR spectra of $A\beta_{14-23}$ fibrils with uniform ^{13}C and ^{15}N labeling of L17 and F20 (*a*), V18 and A21 (*b*), V18 and F20 (*c*), and L17 and A21 (*d*). Spectra were recorded at a ^{13}C NMR frequency of 150.7 MHz, with MAS frequencies of ~20 kHz and between 64 and 256 scans.

line-widths include variations in backbone torsion angles within the β-strand segments by $\sim\pm10°$, variations in side-chain conformations, disorder at the extreme N- and C termini of $A\beta_{14-23}$, variations in contacts between the fine filaments that presumably comprise the fibrils shown in Fig. 1, and variations in the number of or contacts between β-sheet layers within these filaments. When compared with the 2–3 ppm line-widths observed in ^{13}C MAS NMR spectra of other noncrystalline systems, including peptide/antibody complexes (63,64) and helical proteins (65–67) in frozen solutions as well as other amyloid fibrils (17,21,22), the line-widths in Fig. 3 indicate a high degree of structural order, but without true crystallinity.

In solid-state MAS NMR studies of microcrystalline proteins, ^{13}C NMR line-widths <1 ppm are commonly observed at moderate temperatures (68–70). The line-widths increase substantially at low temperatures, where solvent within the crystal is immobilized and protein motions are quenched (71), although crystalline order is not lost. We infer from the ^{13}C NMR line-widths that the level of molecular conformational order in $A\beta_{14-23}$ fibrils is similar to, but not as high, as in microcrystalline proteins because ^{13}C NMR lines for hydrated $A\beta_{14-23}$ fibrils are not as narrow as ^{13}C NMR lines for microcrystalline proteins. Hydrated amyloid fibrils formed by the HET-s protein of *Podospora anserina* have been shown by Siemer et al. to exhibit NMR line-widths on the order of 0.1 ppm (26), possibly because HET-s fibrils are responsible for an evolved biological function (namely, heterokaryon incompatibility (72)) and therefore have a highly homogeneous molecular structure.

Fig. 4 shows 2D-PME spectra of the four $A\beta_{14-23}$ fibril samples. In the 2D-PME spectrum of 18,21-$A\beta_{14-23}$ fibrils, strong crosspeaks (25% of diagonal peaks) are observed between C_α NMR lines of V18 and A21. C_α/C_α crosspeaks are not observed above the noise level in any of the other 2D-PME spectra. This result implies that $A\beta_{14-23}$ fibrils contain antiparallel β-sheets in which V18 aligns with A21, i.e., antiparallel β-sheets with $17+k \leftrightarrow 22-k$ hydrogen-bond registry. C_α/C_α crosspeak intensities for 18,21-$A\beta_{14-23}$ fibrils, relative to diagonal peak intensities, are approximately the same as in previously reported 2D-PME spectra of $A\beta_{16-22}$ and $A\beta_{11-25}$ fibrils for the C_α pairs that are aligned in antiparallel β-sheets in these fibrils (19,58). For example, under quite similar experimental conditions, C_α/C_α crosspeaks for V18/F20 and L17/A21 pairs in 2D-PME spectra of $A\beta_{16-22}$ fibrils (which have $17+k \leftrightarrow 21-k$ registry (10)) were found to have 28% of the volume of V18 and A21 C_α diagonal peaks (58). The observed crosspeak intensities for 18,21-$A\beta_{14-23}$ fibrils indicate that all V18 and A21 residues in $A\beta_{14-23}$ fibrils participate in the $17+k \leftrightarrow 22-k$ registry. Any putative alternations in registry (e.g., as previously suggested for $A\beta_{34-42}$ fibrils (12)) or alternations between antiparallel and parallel β-sheet alignments would reduce the V18/A21 crosspeak intensities by at least a factor of two. Structures with alternating registry or alignment would also necessarily contain two or more inequivalent environments for $A\beta_{14-23}$ molecules (i.e., more than one molecule in the asymmetric unit), potentially splitting each ^{13}C NMR line into two or more components. No splittings are observed in the one- or two-dimensional spectra of $A\beta_{14-23}$ fibrils.

The absence of detectable C_α/C_α crosspeaks in the 2D-PME spectra of 18,20-$A\beta_{14-23}$ and 17,21-$A\beta_{14-23}$ fibrils

TABLE 1 ^{13}C NMR chemical shifts in $A\beta_{14-23}$ fibrils

Residue	CO	C_α	C_β	C_γ	C_δ
L17	172.8 (175.9)	53.3 (53.4)	44.5 (40.7)	24.7 (25.2)	23.8 (23.2, 21.6)
V18	169.8 (174.6)	59.2 (60.5)	34.1 (31.2)	19.6 (19.4, 18.6)	
F20	169.5 (174.1)	54.0 (56.0)	43.0 (37.9)	136.5 (137.2)	
A21	172.5 (176.1)	48.6 (50.8)	21.4 (17.4)		

Values are in ppm relative to tetramethylsilane, based on an external reference of 177.95 ppm for the carboxylate line of polycrystalline L-alanine. Values in parentheses are random coil chemical shifts, taken from Wishart et al. (62) and adjusted to the tetramethylsilane reference by subtraction of 1.7 ppm.

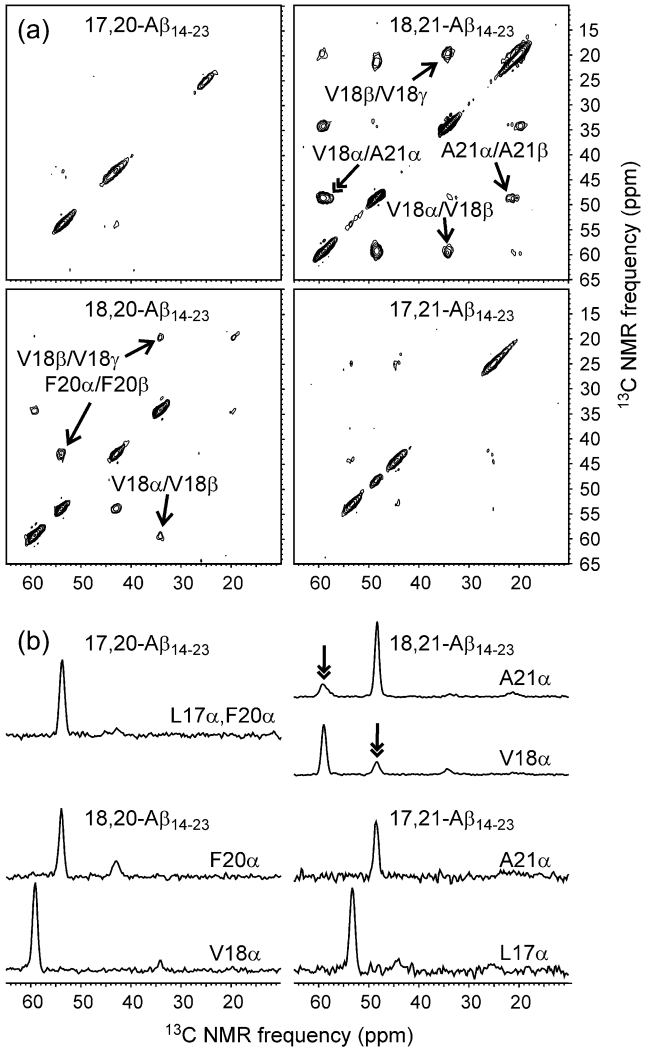

FIGURE 4 (*a*) Aliphatic regions of 2D-PME spectra of lyophilized A$\beta_{14\text{-}23}$ fibrils with the indicated labeled residues. Single-headed arrows indicate assignments of certain intraresidue crosspeaks. Double-headed arrow indicates an interresidue crosspeak. (*b*) One-dimensional slices at the indicated C_α chemical shifts. Double-headed arrows indicate the only interresidue crosspeaks observed in these measurements. Spectra were recorded in 24–72 h, using recycle delays of 2 s and maximum t_1 periods of 3.8 ms.

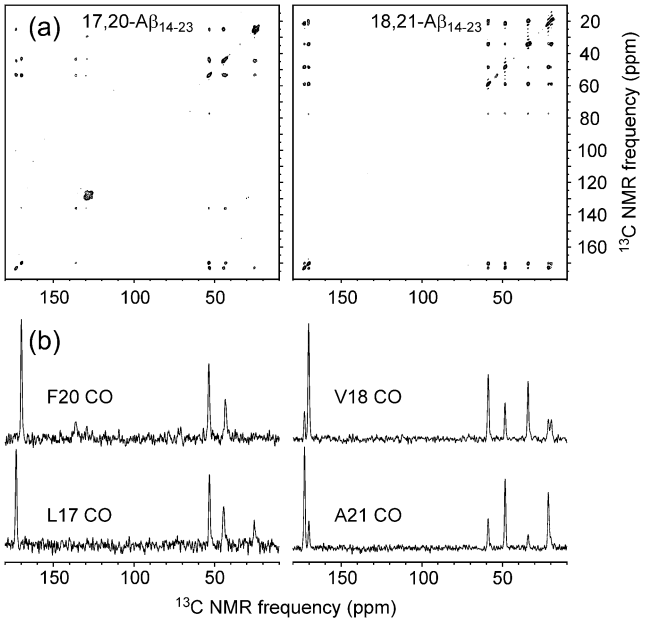

FIGURE 5 (*a*) 2D-RPME spectra of rehydrated A$\beta_{14\text{-}23}$ fibrils with the indicated labeled residues. (*b*) One-dimensional slices at the indicated CO chemical shifts. Spectra were recorded in 48–72 h, using recycle delays of 1.6 s and maximum t_1 periods of 2.3 ms.

places a constraint on the levels of certain defects in the antiparallel β-sheets. In particular, defects that produce $17+k \leftrightarrow 21-k$ alignments cannot be present at levels above 10%. This upper limit on defect concentration is dictated by the signal/noise ratio in the 2D-PME spectra.

Fig. 5 shows 2D-RPME spectra of 17,20-A$\beta_{14\text{-}23}$ and 18,21-A$\beta_{14\text{-}23}$ fibrils. As explained above, the 2D-RPME technique allows hydrogen-bond registry to be investigated in cases where the C_α NMR lines are not resolved. The 2D-RPME spectrum of 17,20-A$\beta_{14\text{-}23}$ shows only intraresidue crosspeaks, including crosspeaks between the CO line of L17 (172.8 ppm) and aliphatic carbon lines of L17 (53.3, 44.5, and 24.7 ppm) and crosspeaks between the CO line of F20 (169.5 ppm) and aliphatic lines of F20 (54.0 and 43.0 ppm). In contrast, the 2D-RPME spectrum of 18,21-A$\beta_{14\text{-}23}$ fibrils shows both intraresidue and interresidue crosspeaks, including crosspeaks between the CO line of V18 and the CO line of A21, crosspeaks between the CO line of V18 and aliphatic lines of A21, and crosspeaks between the CO line of A21 and aliphatic lines of V18. Although the signal/noise ratio is higher in the 2D-RPME spectrum of 18,21-A$\beta_{14\text{-}23}$ fibrils (due to a larger sample quantity), the signal/noise ratio in the 2D-RPME spectrum of 17,20-A$\beta_{14\text{-}23}$ fibrils is high enough to permit the observation of interresidue crosspeaks if they were present. The data in Fig. 5 confirm the $17+k \leftrightarrow 22-k$ hydrogen-bond registry in A$\beta_{14\text{-}23}$ fibrils. In addition, these data demonstrate the utility of the 2D-RPME technique in structural investigations of amyloid fibrils.

Comparison of the 2D-PME and 2D-RPME data for 18,21-A$\beta_{14\text{-}23}$ (Figs. 4 and 5) indicates that the total ^{13}C NMR signal amplitude in the 2D-RPME spectrum (i.e., the integrated signal in the first one-dimensional spectrum, at $t_1 = 0$) is ~25% greater in the 2D-RPME measurement for the same number of scans. Each interresidue crosspeak in the 2D-RPME spectrum has ~15–30% of the volume of the interresidue C_α/C_α crosspeaks in the 2D-PME spectrum.

DISCUSSION

Summary of experimental findings

EM and AFM images in Fig. 1 demonstrate that A$\beta_{14\text{-}23}$ forms amyloid fibrils, as observed previously for many other fragments

of the Alzheimer's β-amyloid peptide (10,12,13,19). As in the case of fibrils formed by other short fragments (10,19), the fibril widths exceed the maximum length of a single peptide chain, suggesting that the observed fibrils are comprised of multiple finer filaments that cannot be resolved in the images. One-dimensional ^{13}C NMR spectra of isotopically labeled A$\beta_{14\text{-}23}$ fibrils in Fig. 3 indicate a high degree of structural order at the molecular level. ^{13}C NMR chemical shifts indicate that residues 17–21 form a continuous β-strand. The 2D-PME and 2D-RPME spectra in Figs. 4 and 5 show that the β-sheets are of the antiparallel type, with a registry that produces a distance <3 Å between H_α sites of V18 and A21. Given the β-strand conformation of residues 17–21, this must be an intermolecular distance. Only $17+k \leftrightarrow 22-k$ registry is consistent with the data. Any alternation in registry or alignment within the β-sheets would be inconsistent with the intensity of C_α-C_α crosspeaks in the 2D-PME spectrum of 18,21-A$\beta_{14\text{-}23}$ fibrils and the absence of splittings of any ^{13}C NMR lines. A molecular model for the antiparallel β-sheets in A$\beta_{14\text{-}23}$ fibrils is shown in Fig. 6.

Antiparallel β-sheets have been established by previous solid-state NMR measurements on A$\beta_{11\text{-}25}$ (19), A$\beta_{16\text{-}22}$ (10) and A$\beta_{34\text{-}42}$ (12) fibrils. The registry in A$\beta_{16\text{-}22}$ fibrils prepared at pH 7.4 is $17+k \leftrightarrow 21-k$, while the registry in A$\beta_{11\text{-}25}$ fibrils is $17+k \leftrightarrow 20-k$ at pH 7.4 and $17+k \leftrightarrow 22-k$ at pH 2.4. Thus, the β-sheet structure in A$\beta_{14\text{-}23}$ fibrils prepared at pH 4.35 is the same as in A$\beta_{11\text{-}25}$ fibrils prepared at low pH.

As observed in solid-state NMR studies of amyloid fibrils formed by other peptides (19,20,73), ^{13}C NMR chemical shifts in lyophilized and hydrated A$\beta_{14\text{-}23}$ fibrils are indistinguishable, indicating that the molecular structure is not affected significantly by hydration. Hydration produces a reduction in ^{13}C NMR line-widths, also as previously observed. From a practical standpoint, lyophilized samples have the advantages of permitting the use of high MAS frequencies, as required for certain solid-state NMR measurements (74–76), and small sample volumes, which in turn permit high rf fields and high sensitivity. Lyophilized samples are not prone to rf-induced heating and to NMR probe tuning instabilities. On the other hand, hydrated samples may be preferred in experiments where the highest possible spectral resolution is required. Similar line-widths have been observed in spectra of samples that are fully hydrated without prior lyophilization (19) and in spectra of samples that were lyophilized and subsequently rehydrated (20,73).

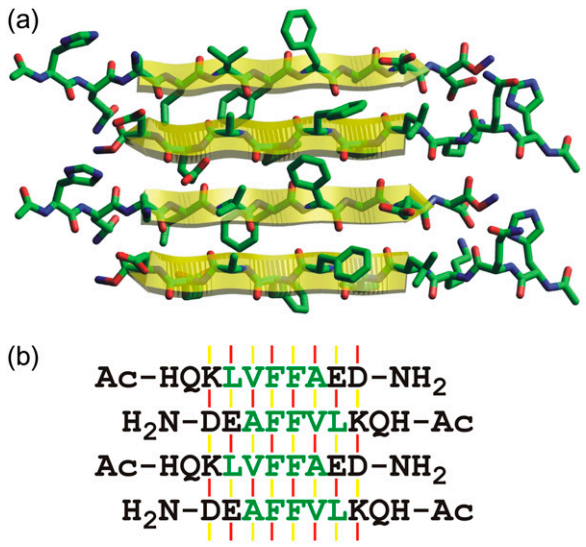

FIGURE 6 (*a*) Molecular model for an antiparallel β-sheet in A$\beta_{14\text{-}23}$ fibrils, with the registry of backbone hydrogen bonds indicated by the solid-state NMR data in Figs. 4 and 5. (*b*) One-letter-code representation, showing hydrogen-bonded (*red lines*) and non-hydrogen-bonded (*yellow lines*) interstrand alignments of amino-acid pairs. Two different sets of alignments (i.e., patterns of *red* and *yellow lines*) alternate along the hydrogen-bonding direction of the antiparallel β-sheet, making two distinct contributions to the calculated free energy.

Theoretical predictions

We now compare the experimental results with theoretical predictions of hydrogen-bond registry in antiparallel β-sheets. These predictions were made in advance of the experiments and were used to select the isotopic labeling patterns and solid-state NMR strategies described above.

The relative probability of a given registry can be estimated from the probability that such an alignment occurs in known protein structures (54). This probability is calculated from the relative probability that individual pairs of residues align in an antiparallel β-sheet in known protein structures, which we take from the database of Wouters and Curmi (77,78). Specifically, Wouters and Curmi report pair-correlation values C^{ij}_{HB} and C^{ij}_{NHB} for all pairs of amino acids i and j, representing the ratio of the observed occurrence of i and j in positions of interstrand alignment (in a set of 253 nonredundant protein structures) to the predicted occurrence of i and j in positions of interstrand alignment if all amino acids in the antiparallel β-sheets were randomly distributed (77). Wouters and Curmi distinguish between hydrogen-bonded (HB) and non-hydrogen-bonded (NHB) alignments, which they find to have significantly different pair correlation values. We calculate the relative probability for a given registry of a given peptide sequence in antiparallel β-sheets in an amyloid fibril by multiplying the relevant C^{ij}_{HB} and C^{ij}_{NHB} values for all aligned residue pairs in that registry. Residues that are unpaired in a given registry (i.e., dangling residues) are assigned a pair correlation value of 1. If the calculated probability is denoted by P, the relative free energy of binding for a given peptide registry is then given by $\Delta G = -RT \ln(P)$, where T is the temperature and R is the gas constant.

Note that each aligned residue pair occurs with both HB and NHB alignments in the antiparallel β-sheets under consideration here, because all β-strands have the same amino-acid sequence and because we consider only β-sheet structures with maximal symmetry. Therefore, we must evaluate two alignment probabilities (for the two combinations of HB and

NHB alignments that alternate along the hydrogen-bonding direction of the β-sheet; see Fig. 6 *b* and accompanying caption for clarification) and two free energies. The final free energy is taken to be the average of the two.

Fig. 7 shows this free energy as a function of the offset N, defined by requiring that residue $17+k$ be aligned with residue $N-k$ of neighboring peptide chains in the β-sheet. For $A\beta_{14\text{-}23}$, the solid-state NMR results indicate that $N = 22$, so that V18 aligns with A21. Solid-state NMR data indicate that $N = 21$ for $A\beta_{16\text{-}22}$ fibrils grown at pH 7.4, while for $A\beta_{11\text{-}25}$ fibrils, $N = 20$ at pH 7.4 and $N = 22$ at pH 2.4. Calculated free energies predict $N = 21$ for all three peptides. In all three cases, the experimental offset is within a deep minimum of the predicted relative free energy. Thus, this simple predictive scheme may be useful to guide experimental design (for instance, by suggesting which residues should be isotopically labeled for solid-state NMR investigations), but does not capture all factors that determine the precise hydrogen-bond registries.

It is interesting to note that the offset required for all residues to participate in an antiparallel β-sheet (i.e., to have no dangling residues) is 21 for $A\beta_{16\text{-}22}$, but 20 for $A\beta_{14\text{-}23}$ and 19 for $A\beta_{11\text{-}25}$. Thus, if one were to attempt to improve the calculation by adding a free energy contribution biased against the number of dangling residues, one could improve the prediction in the case of $A\beta_{11\text{-}25}$ fibrils at pH 7.4 but would worsen it in the other two cases.

We have also used the pair-information values $P_{i,j+m}$ introduced by Steward and Thornton (79) to evaluate the relative probabilities of various registries, as previously described by Petkova et al. (19) The pair-information values take into account interstrand interactions between residues that are not directly aligned. For a given registry, we evaluate the sum of $P_{i,j+m}$ values for $m = -1$, 0, and 1 (i.e., directly aligned residue pairs, and pairs that are shifted by one residue in either direction) and for i being residues 17, 18, 19, 20, and 21. $P_{i,j+m}$ values for hydrogen-bonded and non-hydrogen-bonded pairs i and j are added together, because both types of pairing are present for each residue in the β-sheet structures under consideration. Total information scores are 450, 795, 1042, and 576 for N equal to 19, 20, 21, and 22, respectively. Replacing Asp by Asn and Glu by Gln to approximate the effects of low pH, the total scores become 450, 895, 1036, and 653. If we set $P_{i,j+m} = 0$, so that only directly aligned residues are considered, the scores are 80, 412, 631, and 204 at neutral pH, and 80, 412, 631, and 416 at low pH. Thus, the most likely registry according to the pair-information value treatment is always $17+k \leftrightarrow 21-k$, in agreement with the free energy calculations in Fig. 7.

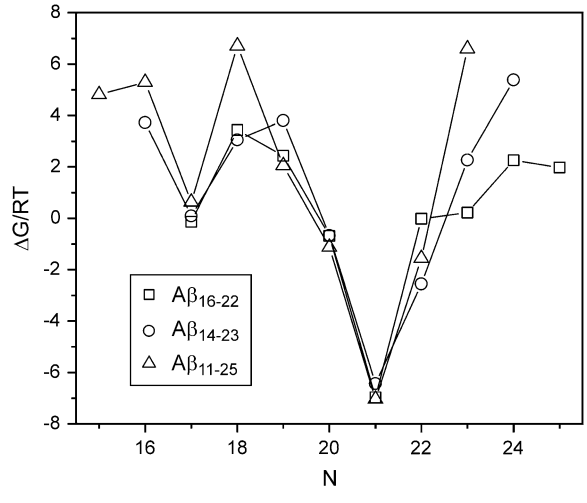

FIGURE 7 Calculated free energies $\Delta G/RT$ as a function of the offset N in antiparallel β-sheets with $17+k \leftrightarrow N-k$ registry, plotted for the three peptides $A\beta_{16\text{-}22}$, $A\beta_{14\text{-}23}$, and $A\beta_{11\text{-}25}$. See text for details of calculations.

More sophisticated and accurate schemes could be formulated by including structural effects or energetics derived from other experimental techniques (80). The approaches described above do not take into account interactions between β-sheet layers, which have been elucidated experimentally in $A\beta_{1\text{-}40}$ fibrils (81) and GNNQQNY fibrils (30), but not in the fibrils discussed above. In $A\beta_{14\text{-}23}$ and $A\beta_{11\text{-}25}$ fibrils, it is not yet known whether residues at the N- and C-termini are structurally ordered and participate in the antiparallel β-sheets. The $17+k \leftrightarrow 22-k$ registry observed in $A\beta_{14\text{-}23}$ fibrils necessarily leaves H14 and Q15 unpaired and outside the β-sheets. Entropy associated with these residues may favor the observed registry over the predicted $17+k \leftrightarrow 21-k$ registry. In addition, the $17+k \leftrightarrow 22-k$ registry results in antiparallel β-sheets with two equivalent faces. Side chains of F19 and F20 create continuous rows of aromatic rings on each face, as shown in Fig. 6. These and other features may be advantageous from the standpoint of interactions between β-sheet layers.

This work was supported by the Intramural Research Program of the National Institute of Diabetes and Digestive and Kidney Diseases, National Institutes of Health, and by a grant to D.J.E.C. from the Alzheimer's Association. Development of solid-state NMR methodology was supported by a grant to R.T. from the Intramural AIDS Targeted Antiviral Program of the National Institutes of Health.

REFERENCES

1. Sacchettini, J. C., and J. W. Kelly. 2002. Therapeutic strategies for human amyloid diseases. *Nat. Rev. Drug Discov.* 1:267–275.
2. Dobson, C. M. 2003. Protein folding and misfolding. *Nature*. 426:884–890.
3. Reches, M., and E. Gazit. 2003. Casting metal nanowires within discrete self-assembled peptide nanotubes. *Science*. 300:625–627.
4. Scheibel, T., R. Parthasarathy, G. Sawicki, X. M. Lin, H. Jaeger, and S. L. Lindquist. 2003. Conducting nanowires built by controlled self-assembly of amyloid fibers and selective metal deposition. *Proc. Natl. Acad. Sci. USA*. 100:4527–4532.
5. Wood, S. J., L. MacKenzie, B. Maleeff, M. R. Hurle, and R. Wetzel. 1996. Selective inhibition of Aβ fibril formation. *J. Biol. Chem.* 271: 4086–4092.
6. Cairo, C. W., A. Strzelec, R. M. Murphy, and L. L. Kiessling. 2002. Affinity-based inhibition of β-amyloid toxicity. *Biochemistry*. 41: 8620–8629.

7. Gordon, D. J., K. L. Sciarretta, and S. C. Meredith. 2001. Inhibition of β-amyloid(40) fibrillogenesis and disassembly of β-amyloid(40) fibrils by short β-amyloid congeners containing *N*-methyl amino acids at alternate residues. *Biochemistry.* 40:8237–8245.
8. Antzutkin, O. N., R. D. Leapman, J. J. Balbach, and R. Tycko. 2002. Supramolecular structural constraints on Alzheimer's β-amyloid fibrils from electron microscopy and solid state nuclear magnetic resonance. *Biochemistry.* 41:15436–15450.
9. Antzutkin, O. N., J. J. Balbach, R. D. Leapman, N. W. Rizzo, J. Reed, and R. Tycko. 2000. Multiple quantum solid state NMR indicates a parallel, not antiparallel, organization of β-sheets in Alzheimer's β-amyloid fibrils. *Proc. Natl. Acad. Sci. USA.* 97:13045–13050.
10. Balbach, J. J., Y. Ishii, O. N. Antzutkin, R. D. Leapman, N. W. Rizzo, F. Dyda, J. Reed, and R. Tycko. 2000. Amyloid fibril formation by $A\beta_{16-22}$, a seven-residue fragment of the Alzheimer's β-amyloid peptide, and structural characterization by solid state NMR. *Biochemistry.* 39:13748–13759.
11. Griffiths, J. M., T. T. Ashburn, M. Auger, P. R. Costa, R. G. Griffin, and P. T. Lansbury. 1995. Rotational resonance solid state NMR elucidates a structural model of pancreatic amyloid. *J. Am. Chem. Soc.* 117:3539–3546.
12. Lansbury, P. T., P. R. Costa, J. M. Griffiths, E. J. Simon, M. Auger, K. J. Halverson, D. A. Kocisko, Z. S. Hendsch, T. T. Ashburn, R. G. S. Spencer, B. Tidor, and R. G. Griffin. 1995. Structural model for the β-amyloid fibril based on interstrand alignment of an antiparallel-sheet comprising a C-terminal peptide. *Nat. Struct. Biol.* 2:990–998.
13. Benzinger, T. L. S., D. M. Gregory, T. S. Burkoth, H. Miller-Auer, D. G. Lynn, R. E. Botto, and S. C. Meredith. 1998. Propagating structure of Alzheimer's β-amyloid$_{10-35}$ is parallel β-sheet with residues in exact register. *Proc. Natl. Acad. Sci. USA.* 95:13407–13412.
14. Gregory, D. M., T. L. S. Benzinger, T. S. Burkoth, H. Miller-Auer, D. G. Lynn, S. C. Meredith, and R. E. Botto. 1998. Dipolar recoupling NMR of biomolecular self-assemblies: determining inter- and intrastrand distances in fibrilized Alzheimer's β-amyloid peptide. *Solid State Nucl. Magn. Reson.* 13:149–166.
15. Benzinger, T. L. S., D. M. Gregory, T. S. Burkoth, H. Miller-Auer, D. G. Lynn, R. E. Botto, and S. C. Meredith. 2000. Two-dimensional structure of β-amyloid$_{10-35}$ fibrils. *Biochemistry.* 39:3491–3499.
16. Burkoth, T. S., T. L. S. Benzinger, V. Urban, D. M. Morgan, D. M. Gregory, P. Thiyagarajan, R. E. Botto, S. C. Meredith, and D. G. Lynn. 2000. Structure of the β-amyloid$_{10-35}$ fibril. *J. Am. Chem. Soc.* 122: 7883–7889.
17. Balbach, J. J., A. T. Petkova, N. A. Oyler, O. N. Antzutkin, D. J. Gordon, S. C. Meredith, and R. Tycko. 2002. Supramolecular structure in full-length Alzheimer's β-amyloid fibrils: evidence for a parallel β-sheet organization from solid state nuclear magnetic resonance. *Biophys. J.* 83:1205–1216.
18. Antzutkin, O. N., J. J. Balbach, and R. Tycko. 2003. Site-specific identification of non-β-strand conformations in Alzheimer's β-amyloid fibrils by solid state NMR. *Biophys. J.* 84:3326–3335.
19. Petkova, A. T., G. Buntkowsky, F. Dyda, R. D. Leapman, W. M. Yau, and R. Tycko. 2004. Solid state NMR reveals a pH-dependent antiparallel β-sheet registry in fibrils formed by a β-amyloid peptide. *J. Mol. Biol.* 335:247–260.
20. Chan, J. C. C., N. A. Oyler, W. M. Yau, and R. Tycko. 2005. Parallel β-sheets and polar zippers in amyloid fibrils formed by residues 10–39 of the yeast prion protein Ure2p. *Biochemistry.* 44:10669–10680.
21. Petkova, A. T., R. D. Leapman, Z. H. Guo, W. M. Yau, M. P. Mattson, and R. Tycko. 2005. Self-propagating, molecular-level polymorphism in Alzheimer's β-amyloid fibrils. *Science.* 307:262–265.
22. Petkova, A. T., Y. Ishii, J. J. Balbach, O. N. Antzutkin, R. D. Leapman, F. Delaglio, and R. Tycko. 2002. A structural model for Alzheimer's β-amyloid fibrils based on experimental constraints from solid state NMR. *Proc. Natl. Acad. Sci. USA.* 99:16742–16747.
23. Jaroniec, C. P., C. E. MacPhee, N. S. Astrof, C. M. Dobson, and R. G. Griffin. 2002. Molecular conformation of a peptide fragment of transthyretin in an amyloid fibril. *Proc. Natl. Acad. Sci. USA.* 99:16748–16753.
24. Jaroniec, C. P., C. E. MacPhee, V. S. Bajaj, M. T. McMahon, C. M. Dobson, and R. G. Griffin. 2004. High-resolution molecular structure of a peptide in an amyloid fibril determined by magic-angle-spinning NMR spectroscopy. *Proc. Natl. Acad. Sci. USA.* 101:711–716.
25. Ritter, C., M. L. Maddelein, A. B. Siemer, T. Luhrs, M. Ernst, B. H. Meier, S. J. Saupe, and R. Riek. 2005. Correlation of structural elements and infectivity of the HET-s prion. *Nature.* 435:844–848.
26. Siemer, A. B., C. Ritter, M. Ernst, R. Riek, and B. H. Meier. 2005. High-resolution solid state NMR spectroscopy of the prion protein HET-s in its amyloid conformation. *Angew. Chem. Int. Ed. Engl.* 44:2441–2444.
27. Eanes, E. D., and G. G. Glenner. 1968. X-ray diffraction studies on amyloid filaments. *J. Histochem. Cytochem.* 16:673–677.
28. Inouye, H., P. E. Fraser, and D. A. Kirschner. 1993. Structure of β-crystallite assemblies formed by Alzheimer β-amyloid protein analogs: analysis by x-ray diffraction. *Biophys. J.* 64:502–519.
29. Sunde, M., L. C. Serpell, M. Bartlam, P. E. Fraser, M. B. Pepys, and C. C. F. Blake. 1997. Common core structure of amyloid fibrils by synchrotron x-ray diffraction. *J. Mol. Biol.* 273:729–739.
30. Nelson, R., M. R. Sawaya, M. Balbirnie, A. O. Madsen, C. Riekel, R. Grothe, and D. Eisenberg. 2005. Structure of the cross-β spine of amyloid-like fibrils. *Nature.* 435:773–778.
31. Gordon, D. J., J. J. Balbach, R. Tycko, and S. C. Meredith. 2004. Increasing the amphiphilicity of an amyloidogenic peptide changes the β-sheet structure in the fibrils from antiparallel to parallel. *Biophys. J.* 86:428–434.
32. Goldsbury, C., K. Goldie, J. Pellaud, J. Seelig, P. Frey, S. A. Muller, J. Kistler, G. J. S. Cooper, and U. Aebi. 2000. Amyloid fibril formation from full-length and fragments of amylin. *J. Struct. Biol.* 130:352–362.
33. Goldsbury, C. S., S. Wirtz, S. A. Muller, S. Sunderji, P. Wicki, U. Aebi, and P. Frey. 2000. Studies on the in vitro assembly of $A\beta_{1-40}$: implications for the search for Aβ fibril formation inhibitors. *J. Struct. Biol.* 130:217–231.
34. Jimenez, J. L., E. J. Nettleton, M. Bouchard, C. V. Robinson, C. M. Dobson, and H. R. Saibil. 2002. The protofilament structure of insulin amyloid fibrils. *Proc. Natl. Acad. Sci. USA.* 99:9196–9201.
35. Jimenez, J. L., J. L. Guijarro, E. Orlova, J. Zurdo, C. M. Dobson, M. Sunde, and H. R. Saibil. 1999. Cryo-electron microscopy structure of an SH3 amyloid fibril and model of the molecular packing. *EMBO J.* 18:815–821.
36. Serpell, L. C., and J. M. Smith. 2000. Direct visualisation of the β-sheet structure of synthetic Alzheimer's amyloid. *J. Mol. Biol.* 299:225–231.
37. Makin, O. S., E. Atkins, P. Sikorski, J. Johansson, and L. C. Serpell. 2005. Molecular basis for amyloid fibril formation and stability. *Proc. Natl. Acad. Sci. USA.* 102:315–320.
38. Serag, A. A., C. Altenbach, M. Gingery, W. L. Hubbell, and T. O. Yeates. 2002. Arrangement of subunits and ordering of β-strands in an amyloid sheet. *Nat. Struct. Biol.* 9:734–739.
39. Jayasinghe, S. A., and R. Langen. 2004. Identifying structural features of fibrillar islet amyloid polypeptide using site-directed spin labeling. *J. Biol. Chem.* 279:48420–48425.
40. Der-Sarkissian, A., C. C. Jao, J. Chen, and R. Langen. 2003. Structural organization of α-synuclein fibrils studied by site-directed spin labeling. *J. Biol. Chem.* 278:37530–37535.
41. Torok, M., S. Milton, R. Kayed, P. Wu, T. McIntire, C. G. Glabe, and R. Langen. 2002. Structural and dynamic features of Alzheimer's Aβ peptide in amyloid fibrils studied by site-directed spin labeling. *J. Biol. Chem.* 277:40810–40815.
42. Tanaka, M., P. Chien, N. Naber, R. Cooke, and J. S. Weissman. 2004. Conformational variations in an infectious protein determine prion strain differences. *Nature.* 428:323–328.
43. Kheterpal, I., S. Zhou, K. D. Cook, and R. Wetzel. 2000. Aβ amyloid fibrils possess a core structure highly resistant to hydrogen exchange. *Proc. Natl. Acad. Sci. USA.* 97:13597–13601.
44. Hoshino, M., H. Katou, Y. Hagihara, K. Hasegawa, H. Naiki, and Y. Goto. 2002. Mapping the core of the β_2-microglobulin amyloid fibril by H/D exchange. *Nat. Struct. Biol.* 9:332–336.

45. Ippel, J. H., A. Olofsson, J. Schleucher, E. Lundgren, and S. S. Wijmenga. 2002. Probing solvent accessibility of amyloid fibrils by solution NMR spectroscopy. *Proc. Natl. Acad. Sci. USA.* 99:8648–8653.

46. Whittemore, N. A., R. Mishra, I. Kheterpal, A. D. Williams, R. Wetzel, and E. H. Serpersu. 2005. Hydrogen-deuterium (H/D) exchange mapping of Aβ_{1-40} amyloid fibril secondary structure using nuclear magnetic resonance spectroscopy. *Biochemistry.* 44:4434–4441.

47. Olofsson, A., A. E. Sauer-Eriksson, and A. Ohman. 2006. The solvent protection of Alzheimer amyloid-β_{1-42} fibrils as determined by solution NMR spectroscopy. *J. Biol. Chem.* 281:477–483.

48. Shivaprasad, S., and R. Wetzel. 2004. An intersheet packing interaction in Aβ fibrils mapped by disulfide cross-linking. *Biochemistry.* 43: 15310–15317.

49. Kheterpal, I., A. Williams, C. Murphy, B. Bledsoe, and R. Wetzel. 2001. Structural features of the Aβ amyloid fibril elucidated by limited proteolysis. *Biochemistry.* 40:11757–11767.

50. Baxa, U., K. L. Taylor, J. S. Wall, M. N. Simon, N. Q. Cheng, R. B. Wickner, and A. C. Steven. 2003. Architecture of Ure2p prion filaments: the N-terminal domains form a central core fiber. *J. Biol. Chem.* 278:43717–43727.

51. Williams, A. D., E. Portelius, I. Kheterpal, J. T. Guo, K. D. Cook, Y. Xu, and R. Wetzel. 2004. Mapping Aβ amyloid fibril secondary structure using scanning proline mutagenesis. *J. Mol. Biol.* 335:833–842.

52. Williams, A. D., S. Shivaprasad, and R. Wetzel. 2006. Alanine scanning mutagenesis of Aβ_{1-40} amyloid fibril stability. *J. Mol. Biol.* 357: 1283–1294.

53. Shivaprasad, S., and R. Wetzel. 2006. Scanning cysteine mutagenesis analysis of Aβ_{1-40} amyloid fibrils. *J. Biol. Chem.* 281:993–1000.

54. Tjernberg, L. O., A. Tjernberg, N. Bark, Y. Shi, B. P. Ruzsicska, Z. M. Bu, J. Thyberg, and D. J. E. Callaway. 2002. Assembling amyloid fibrils from designed structures containing a significant amyloid β-peptide fragment. *Biochem. J.* 366:343–351.

55. Tjernberg, L. O., D. J. E. Callaway, A. Tjernberg, S. Hahne, C. Lilliehook, L. Terenius, J. Thyberg, and C. Nordstedt. 1999. A molecular model of Alzheimer amyloid β-peptide fibril formation. *J. Biol. Chem.* 274:12619–12625.

56. Pines, A., M. G. Gibby, and J. S. Waugh. 1973. Proton-enhanced NMR of dilute spins in solids. *J. Chem. Phys.* 59:569–590.

57. Bennett, A. E., C. M. Rienstra, M. Auger, K. V. Lakshmi, and R. G. Griffin. 1995. Heteronuclear decoupling in rotating solids. *J. Chem. Phys.* 103:6951–6958.

58. Tycko, R., and Y. Ishii. 2003. Constraints on supramolecular structure in amyloid fibrils from two-dimensional solid state NMR spectroscopy with uniform isotopic labeling. *J. Am. Chem. Soc.* 125:6606–6607.

59. Bennett, A. E., C. M. Rienstra, J. M. Griffiths, W. G. Zhen, P. T. Lansbury, and R. G. Griffin. 1998. Homonuclear radio-frequency-driven recoupling in rotating solids. *J. Chem. Phys.* 108:9463–9479.

60. Gullion, T., and S. Vega. 1992. A simple magic-angle spinning NMR experiment for the dephasing of rotational echoes of dipolar coupled homonuclear spin pairs. *Chem. Phys. Lett.* 194:423–428.

61. Gullion, T., D. B. Baker, and M. S. Conradi. 1990. New, compensated Carr-Purcell sequences. *J. Magn. Reson.* 89:479–484.

62. Wishart, D. S., C. G. Bigam, A. Holm, R. S. Hodges, and B. D. Sykes. 1995. ^{1}H, ^{13}C and ^{15}N random coil NMR chemical shifts of the common amino acids. 1. Investigations of nearest-neighbor effects. *J. Biomol. NMR.* 5:67–81.

63. Sharpe, S., N. Kessler, J. A. Anglister, W. M. Yau, and R. Tycko. 2004. Solid state NMR yields structural constraints on the V3 loop from HIV-1 gp120 bound to the 447–52d antibody Fv fragment. *J. Am. Chem. Soc.* 126:4979–4990.

64. Weliky, D. P., A. E. Bennett, A. Zvi, J. Anglister, P. J. Steinbach, and R. Tycko. 1999. Solid state NMR evidence for an antibody-dependent conformation of the V3 loop of HIV-1 gp120. *Nat. Struct. Biol.* 6: 141–145.

65. Blanco, F. J., S. Hess, L. K. Pannell, N. W. Rizzo, and R. Tycko. 2001. Solid state NMR data support a helix-loop-helix structural model for the N-terminal half of HIV-1 Rev in fibrillar form. *J. Mol. Biol.* 313: 845–859.

66. Long, H. W., and R. Tycko. 1998. Biopolymer conformational distributions from solid state NMR: α-helix and 3_{10}-helix contents of a helical peptide. *J. Am. Chem. Soc.* 120:7039–7048.

67. Havlin, R. H., and R. Tycko. 2005. Probing site-specific conformational distributions in protein folding with solid state NMR. *Proc. Natl. Acad. Sci. USA.* 102:3284–3289.

68. Castellani, F., B. J. van Rossum, A. Diehl, K. Rehbein, and H. Oschkinat. 2003. Determination of solid state NMR structures of proteins by means of three-dimensional ^{15}N-^{13}C-^{13}C dipolar correlation spectroscopy and chemical shift analysis. *Biochemistry.* 42:11476–11483.

69. Franks, W. T., D. H. Zhou, B. J. Wylie, B. G. Money, D. T. Graesser, H. L. Frericks, G. Sahota, and C. M. Rienstra. 2005. Magic-angle spinning solid state NMR spectroscopy of the β1 immunoglobulin binding domain of protein G (GB1): ^{15}N and ^{13}C chemical shift assignments and conformational analysis. *J. Am. Chem. Soc.* 127:12291–12305.

70. Igumenova, T. I., A. E. McDermott, K. W. Zilm, R. W. Martin, E. K. Paulson, and A. J. Wand. 2004. Assignments of carbon NMR resonances for microcrystalline ubiquitin. *J. Am. Chem. Soc.* 126:6720–6727.

71. Martin, R. W., and K. W. Zilm. 2003. Preparation of protein nanocrystals and their characterization by solid state NMR. *J. Magn. Reson.* 165:162–174.

72. Coustou, V., C. Deleu, S. Saupe, and J. Begueret. 1997. The protein product of the *het-s* heterokaryon incompatibility gene of the fungus *Podospora anserina* behaves as a prion analog. *Proc. Natl. Acad. Sci. USA.* 94:9773–9778.

73. Paravastu, A. K., A. T. Petkova, and R. Tycko. 2006. Polymorphic fibril formation by residues 10–40 of the Alzheimer's β-amyloid peptide. *Biophys. J.* 90:4618–4629.

74. Ishii, Y., J. J. Balbach, and R. Tycko. 2001. Measurement of dipole-coupled lineshapes in a many-spin system by constant-time two-dimensional solid state NMR with high-speed magic-angle spinning. *Chem. Phys.* 266:231–236.

75. Ishii, Y., and R. Tycko. 2000. Sensitivity enhancement in solid state ^{15}N NMR by indirect detection with high-speed magic-angle spinning. *J. Magn. Reson.* 142:199–204.

76. Ishii, Y., J. P. Yesinowski, and R. Tycko. 2001. Sensitivity enhancement in solid state ^{13}C NMR of synthetic polymers and biopolymers by ^{1}H NMR detection with high-speed magic-angle spinning. *J. Am. Chem. Soc.* 123:2921–2922.

77. Wouters, M. A., and P. M. G. Curmi. 1995. An analysis of side-chain interactions and pair correlations within antiparallel β-sheets: the differences between backbone hydrogen-bonded and non-hydrogen-bonded residue pairs. *Proteins.* 22:119–131.

78. Chu, C. K., L. L. Feng, and M. A. Wouters. 2005. Comparison of sequence and structure-based datasets for nonredundant structural data mining. *Proteins.* 60:577–583.

79. Steward, R. E., and J. M. Thornton. 2002. Prediction of strand pairing in antiparallel and parallel β-sheets using information theory. *Proteins.* 48:178–191.

80. Shi, Y., P. F. W. Stouten, N. Pillalamarri, L. Barile, R. V. Rosal, S. Teichberg, Z. M. Bu, and D. J. E. Callaway. 2006. Quantitative determination of the topological propensities of amyloidogenic peptides. *Biophys. Chem.* 120:55–61.

81. Petkova, A. T., W. M. Yau, and R. Tycko. 2006. Experimental constraints on quaternary structure in Alzheimer's β-amyloid fibrils. *Biochemistry.* 45:498–512.